Available online at www.sciencedirect.com

ScienceDirect

Procedia Engineering 109 (2015) 135 – 143

Procedia Engineering

www.elsevier.com/locate/procedia

XXIII Italian Group of Fracture Meeting, IGFXXIII

Graphite nodules influence on DCIs mechanical properties: experimental and numerical investigation

Vittorio Di Cocco[a], Daniela Iacoviello[b]*, Francesco Iacoviello[a], Alessandra Rossi[a]

[a]*University of Cassino and Southern Lazio - DICeM, via G. Di Biasio 43, 03043, Cassino (FR), Italy*
[b]*University of Rome "Sapienza"- DIIAG "Antonio Ruberti", via Ariosto 25, 00185, Rome, Italy*

Abstract

Ductile cast irons (DCIs) are characterized by very interesting properties, with a good castability (typical of cast irons) and a very interesting mechanical behaviour, that is comparable to low alloyed steels. From the point of view of the microstructure, these alloys can be considered as natural composites, with graphite nodules embedded in a metal matrix. Their mechanical properties are influenced both by the matrix microstructure (e.g., ferrite, pearlite, ferrite-pearlite, austenite, etc.) and by the morphological peculiarities of the graphite elements (nodularity, element distribution, dimensions etc.). In this work, an experimental and numerical procedure has been optimized in order to obtain a 3D representation of a ferritic DCI considering the effective distribution of the graphite elements. Starting from this 3D representation, the behavior of the investigated DCI has been simulated by means of finite elements approach.

Peer-review under responsibility of the Gruppo Italiano Frattura (IGF)

Keywords: Ductile Cast Iron; Microstructure; Graphite nodules.

Nomenclature

DCI	Ductile Cast Iron
VB	Visual Basic

* Corresponding author. Tel.: +39.0677274061.
E-mail address: iacoviello@dis.uniroma1.it

Peer-review under responsibility of the Gruppo Italiano Frattura (IGF)
doi:10.1016/j.proeng.2015.06.223

1. Introduction

Discovered in 1948, Ductile Cast Irons (DCIs) can be considered as ternary Fe-C-Si alloys, characterized by C and Si contents that range between 3.5-3.9% and 1.8-2.8%, respectively. Graphite elements are characterized by a nodule-like shape and their nucleation and growth are influenced by many parameters, like the alloy purity level and the spheroidizing elements addition, like Mg, Ca or rare earth, like Ce or La [1]. Graphite elements can nucleate corresponding to different nucleation sites like gas bubbles or some inclusions (e.g., MgS, CaS, SrS, MgO) [2, 3], and they growth by means of a carbon solid state diffusion mechanism, through the austenite shields around the graphite spherulite. As final result of the solidification and cooling process, DCIs can be considered as a sort of "natural composite" with graphite nodules embedded in a metal matrix. Microstructure strongly influences the DCIs mechanical properties, both considering the graphite nodules morphological peculiarities (e.g., nodularity, dimension, distribution) and considering the matrix phases: ferritic, pearlitic, ferritic-pearlitic, martensitic, austenitic austempered DCIs can be obtained controlling the chemical composition and/or the manufacturing process and/or optimizing heat treatment processes. Damaging micromechanisms are strongly influenced by the loading conditions (e.g., static or quasi static or cyclic or dynamic stress) and by the DCI microstructure [4-9], considering both the matrix phases and the graphite nodules morphological peculiarities. Focussing on ferritic DCI, graphite nodules are often considered as voids embedded in a ductile matrix [4], but more recent analysis [5-9] showed that ferritic matrix-graphite nodules debonding is not the most important damaging micromechanism: due to the presence of a mechanical properties gradient inside the graphite nodules, the initiation and propagation of cracks inside graphite nodules is more often observed (so called "onion like mechanism").

In this work an experimental and numerical procedure was optimized in order to obtain a 3D representation of a ferritic DCI with the effective graphite nodules shape and distribution. A nodule 3D-model was reconstructed by stacking all the collected images. The idea of considering the 3D modelization to better characterize the internal structure of an object (in material science, medicine and so on) has been implemented in the last years due to the development of image processing techniques and software for the 3D reconstruction. Particular attention has been devoted to the reconstruction of complex 3D pore morphologies [10, 11]. The knowledge of the material microstructure and of the spatial distribution of the pores allowed the evaluation of titanium alloy's properties by using section microscopy [12]. The reconstructed 3D microstructure could be useful for a finite element analysis of mechanical response [11]. The mechanical behavior and properties, the Young's modulus, and the stress-strain behavior, of heterogeneous materials could be predicted by the 3D modeling [14]; 2D images were acquired by serial sectioning method and used to reconstruct the 3D microstructure of the material for the finite element analysis. The approach that will be used in this paper is similar to the one just discussed.

The result of this analysis was used to simulate the mechanical behaviour of the investigated DCI considering the effective graphite nodule shape and the presence of an internal gradient of mechanical properties.

2. Investigated material and experimental procedure

2.1. Investigated material

Investigated DCI (GJS 350-22) was characterized by a fully ferritic matrix and by a high graphite elements nodularity (higher than 85%, with a graphite elements volume fraction of about 9-10% and 132 nodules per mm^2; chemical composition is shown in Tab. 1).

Table 1. Investigated ferritic DCI chemical composition.

C	Si	Mn	S	P	Cu	Cr	Mg	Sn
3.62	2.72	0.19	0.011	0.021	0.019	0.041	0.047	0.011

2.2. Experimental procedure

In order to investigate the contours of nodules on the slides pictures, the experimental activity was performed according to the following procedure:

1. Metallographic preparation (up to 1μm diamond powder);
2. Perform one Vickers microhardness indentation and measure the indentation diagonals;
3. Identification of the area to be analyzed by means of a digital microscope (and take a picture of this area);
4. New (light) metallographic preparation (only with 1μm diamond powder), in order to remove a thickness between 1 and 1.5 μm;
5. Perform a measurement of the indentation diagonals: knowing the indenter geometry it is possible to calculate the removed DCI thickness;
6. Observe the same area of stage 3 by means of the digital microscope (and take a picture of this area)
7. Repeat stages 4-6.

According to this procedure, 100 observations were performed of the same area at different level, obtaining 100 slices of the same area to be used in the assembling procedure.

In Fig.1 the images of three slices are presented:

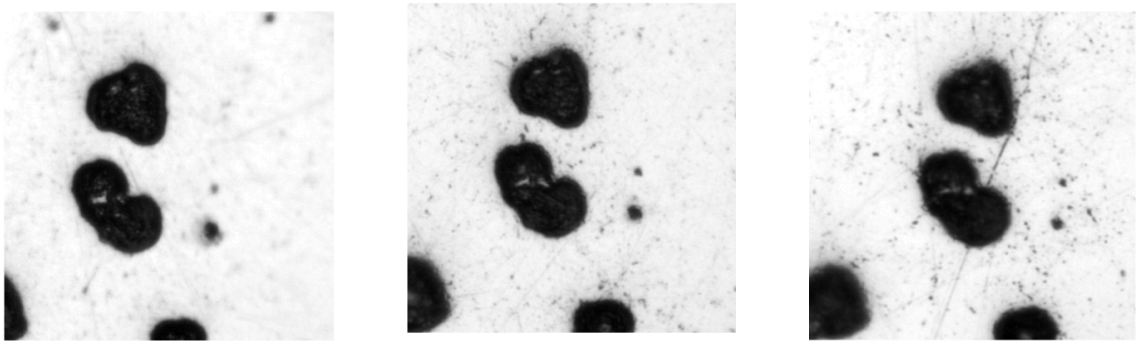

a) b) c)

Fig.1. Three different slices.

2.2.1 The binarization step

Images in Fig. 1 were obtained by successively and uniformly removing slices of the material; the images were available at a spacing of about 1 μm, thus allowing an accurate description of the nodules.
In each image the nodules are recognizable, represented by the darkest elements; nevertheless since also scratches and dust were present, a binarization procedure was adopted to clearly identify just the principal nodules present in each image. The simplest binarization method requires the choice of a threshold; if the histogram of the image presents two distinct peaks representing the objects and the background, the choice of the threshold may be assumed as the separating element between the two peaks. This situation is not very common when dealing with real data, therefore sophisticated methods have been proposed to adequately chose the threshold. Depending on the specific kind of image at hand different techniques were proposed. In Sauvola et al. [15], a survey on documents binarization methods was presented, along with the presentation of an adaptive binarization one. Using automatic double-threshold, common deficiencies of image binarization methods were overcome by using information from the Canny edge detector to obtain high and low threshold [16]. More recently a locally adaptive thresholding technique was proposed in [17]; it is based on the calculus of local mean. If the image presents uniform contrast distribution global thresholding is appropriate. The images considered in this paper were all caught at the same uniform illumination conditions, therefore the well-known Otsu method was adopted [18]; the idea was to find the optimal threshold to separate the dark objects (the nodules) from the background by minimizing a suitable cost index. More precisely, referring to one image, it was assumed that its pixels could be represented by L gray levels, $[1,2,...,L]$; moreover

the set of the pixels was assumed as divided by a threshold at level k in two classes [18]. The pixels with levels $[1,2,...,k]$ belonged to the background C_0 and the pixels with levels $[k+1,...,L]$ to the objects set C_1, or vice versa.

The total number N of pixels could be expressed as

$$N = \sum_{i=1}^{L} n_i$$

where n_i was the number of pixels with gray level equal to i; it is useful to consider the probability distribution:

$$p_i = \frac{n_i}{N} \geq 0 \quad \sum_{i=1}^{L} p_i = 1$$

The probabilities of class occurrence were given by:

$$w_0 = \sum_{i=1}^{k} p_i = w(k)$$

$$w_1 = \sum_{i=1+k}^{L} p_i = 1 - w(k)$$

and the class mean levels were:

$$\mu_0 = \sum_{i=1}^{k} i p_i / w_0 = \mu(k) / w(k)$$

$$\mu_1 = \sum_{i=1+k}^{L} i p_i / w_0 = \frac{\sum_{i=1}^{L} i p_i - \mu(k)}{1 - w(k)} = \frac{\mu_L - \mu(k)}{1 - w(k)}$$

It has been possible to deduce expressions for the class variances:

$$\sigma_0^2 = \sum_{i=1}^{k} (i - \mu_0)^2 p_i / w_0$$

$$\sigma_1^2 = \sum_{i=k+1}^{L} (i - \mu_1)^2 p_i / w_1$$

To determine the optimal threshold cost indices that evaluate the quality of the threshold at level k were introduced:

$$J_1 = \frac{w_0 (\mu_0 - \mu_L)^2 + w_1 (\mu_1 - \mu_L)^2}{w_0 \sigma_0^2 + w_1 \sigma_1^2}$$

that is the within class variance;

$$J_2 = \frac{\sum_{i=1}^{L} \left(i - \mu(L)\right)^2 p_i}{w_0 \sigma_0^2 + w_1 \sigma_1^2}$$

that is the between class variance; and

$$J_3 = \frac{w_0 (\mu_0 - \mu_L)^2 + w_1 (\mu_1 - \mu_L)^2}{\sum_{i=1}^{L} \left(i - \mu(L)\right)^2 p_i}$$

that is the total variance of levels.

Another equivalent criteria was introduced to evaluate the separability capability of the threshold k

$$J = \frac{J_1}{1 + J_1}$$

The optimal threshold should provide the best separation of the two classes C_0 and C_1. The discriminant criteria herein recalled were equivalent one another. The Otsu method could be also extended for multi-threshold problems.

In Fig.2 the binarization of the images of Fig.1 are reported.

a) b) c)

Fig.2. Binarization of the original data of Fig.1 obtained by the Otsu method.

2.2.2 The 3D model

The 3D model of investigated nodule was imported in a commercial FEM software in order to simulate the behavior of graphite in the ferritic matrix. According to previous authors results [7, 9, 19], the nodule was implemented on the FEM as an assembly of two graphite components:

1) The first component of assembly is the nodule outer shield (due to a carbon solid diffusion mechanism);
2) The second component is the nodule core (obtained directly from the melt during the solidification process).

The component core was obtained by means of a scaling procedure of the 3D model (80%), and the nodule shield was obtained as a difference between the 3D model and the nodule core. Finally, the nodule was surrounded by a box of ferritic matrix characterize by dimensions of 3 times the diameter of nodule (about 300 μm).
An isotropic hardening tangent data model was used to characterize the stress strain behavior of matrix, whereas a simply fully elastic behavior with an elastic module of 80 GPa was used to investigate the mechanical behavior of both skin and core of graphite nodule as shown in Tab. 2.

Table 2. Investigated ferritic DCI chemical composition.

Phase	E [GPa]	E_{Tiso} [GPa]	σ_y [MPa	ν
Ferrite	190	80	380	0.3
Graphite	80	---	---	0.2

The mesh was generated by using free tetrahedral elements characterized by minimum size of about 2 μm.

3. Results

3.1. Assembling procedure

In Fig. 3b the result of the binarization obtained by applying the Otsu method is shown considering the slice of Fig. 3a). A simple morphological operations based on area filtering allowed to eliminate some small objects, not related to the nodules, that might be present after the binarization:
Once all the images were binarized according to the procedure recalled in subsection 2.2.1, the contours of the nodules were extracted; see Fig.4 in which the contours of the nodules present in image of Fig.3b were shown.
3D wired model was obtained by using a simple VB code which put the numerical coordinates of contours on a traditional CAD software, as shown in Fig. 5.
Considering the main nodule observed during the experimental procedure, in order to simplify the model, the surrounding nodules were cancelled, obtaining the solid 3D model to be exported in the FEM software (Figs. 6 a and b).

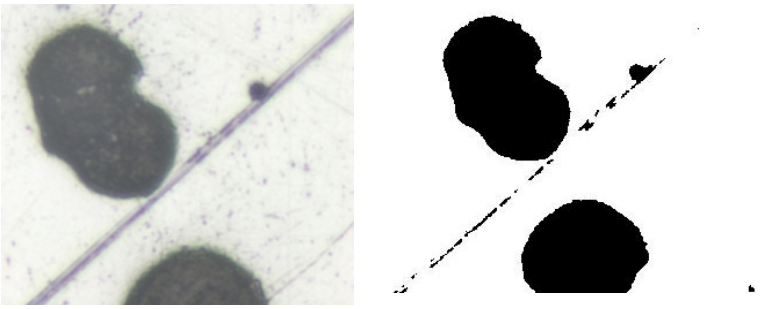

a) b)

Fig. 3. Beginning image processing steps: a) source metallography, b) binarized and filtered result.

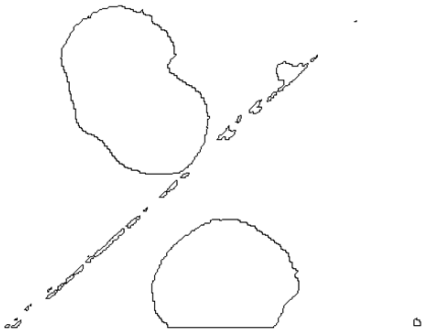

Fig.4. Contours of binarized and filtered image in Fig.2b.

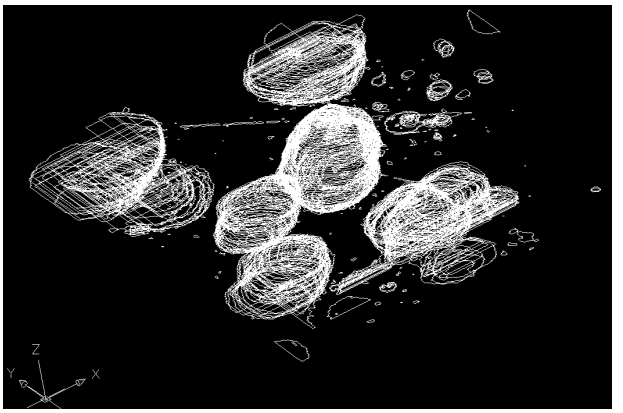

Fig.5. Wired 3D slices reconstruction.

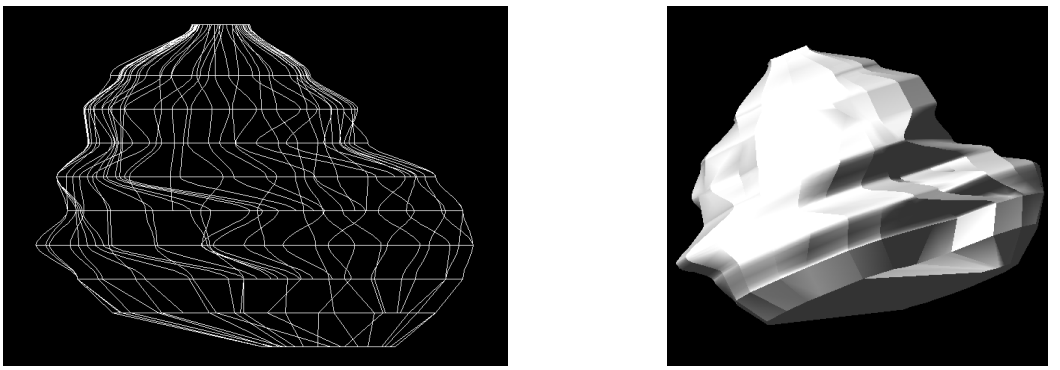

a) b)

Fig. 6: investigated solid 3D model nodule: a) wire representation, b) rendering.

3.2. FEM results

The analysis were performed considering two different conditions:

1) A simply ferritic matrix volume with a hole inside (with the same shape of the 3D nodule);
2) A more realistic microstructure, with a graphite nodule (characterized by the presence of a shield and of a core) embedded in a ferritic matrix; in this case, two interfaces are present: matrix – graphite shield and graphite shield – graphite core; interfaces were modeled as a continuum contacts.

In both investigated conditions, an uniaxial 350MPa load was remotely applied (30 MPa less than the ferrite yield stress).

In the first simulation, the maximum von Mises stress obtained was about 563 MPa; this value is higher than the ferrite yield stress: as a consequence, the presence of hole increases the local stress due to well known stress intensity factor phenomenon (Fig. 7).

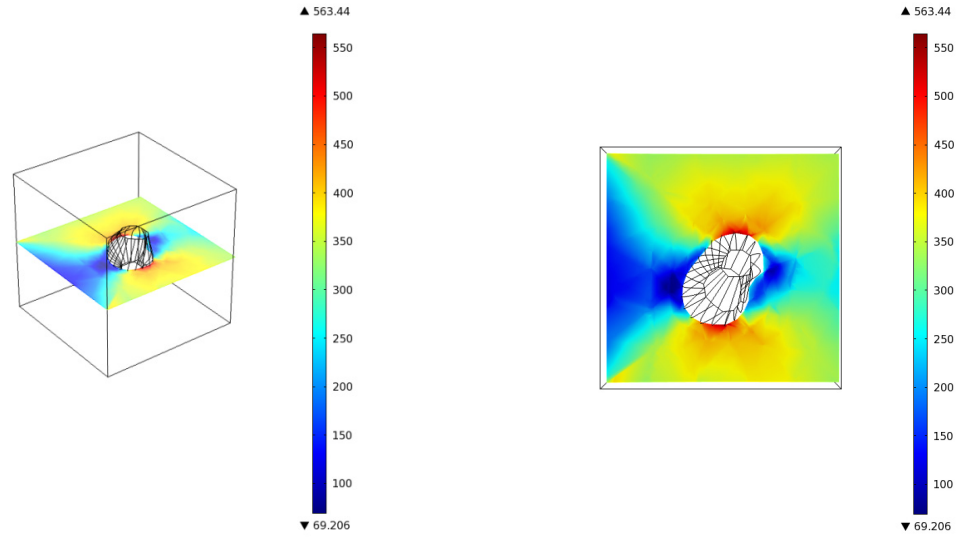

Fig. 7. Von Mises stresses [MPa] around a slice of hole.

Considering the graphite nodule embedded in the ferritic matrix (Fig 8), the maximum von Mises stress value decreases from about 563 MPa to about 471 MPa (always higher than the ferrite yield strength). The graphite nodules presence reduces the maximum stress, due to the interaction between graphite and ferritic matrix.

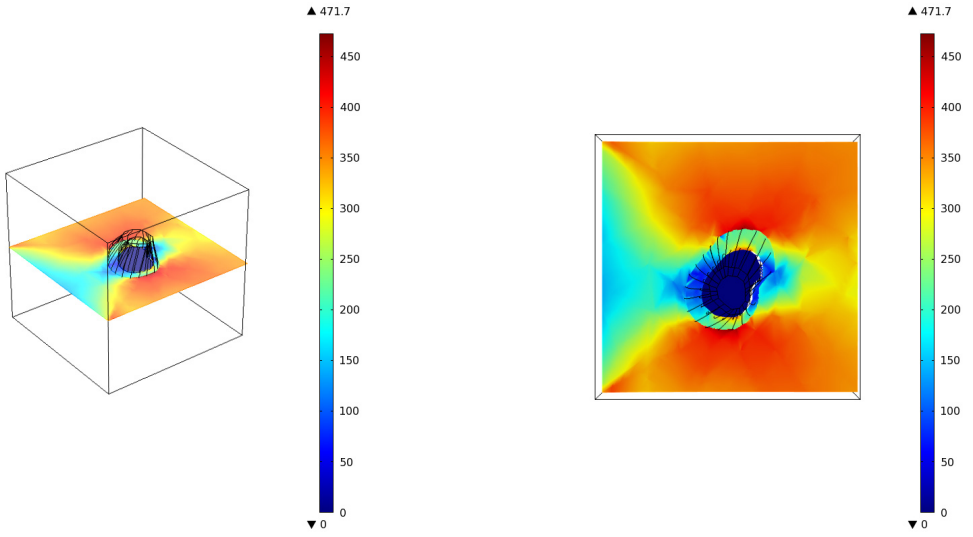

Fig. 8. Von Mises stresses [MPa] around a slice of graphite nodule.

Considering the displacement field on the investigated slice (Fig. 9), an internal debonding at the interface graphite shield - graphite core is observed, although the simulation was performed under the hypothesis of an identical graphite mechanical behavior in the shield and in the core. This behavior agrees with the observed damaging micromechanism (so called “onion-like”). Anyway, preliminary experimental results [7, 9, 19] confirm the presence of an internal mechanical properties gradient inside the graphite nodules. Further analysis will allow to quantitatively define this mechanical properties gradient. New simulations will allow to describe more precisely the phenomenon.

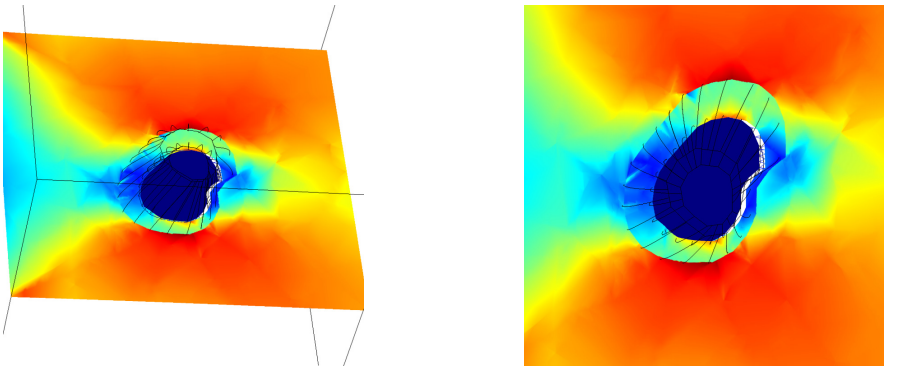

Fig. 9. Displacement field around the investigated nodule slice.

4. Conclusion

In this work a numerical procedure based on image analysis was proposed and applied to generate a 3D model of a nodule embedded in a ferritic DCI. Using a commercial FEM code, the 3D model of the graphite nodule was used to investigate the mechanical effect of graphite in the DCI matrix. Considering the observed damaging miromechanism (internal debonding in graphite elements), the graphite element behavior was simulated hypotizing the presence of an internal interface (between a nodule core, obtained directly from the melt, and a nodule shield, obtained by means of carbon solid diffusion mechanism) and of an “external” surface (between the nodule and the ferritic matrix). According the FEM simulation results, the following conclusions can be summarized:

1) Image analysis allows to obtain a realistic 3D model of the graphite elements in a DCI.
2) Comparing the results obtained with a ferritic matrix with embedded holes and a ferritic matrix with embedded graphite nodules, and applying the same load, the presence of graphite nodules decreases the stress intensification near the graphite elements. As a consequence, ferritic DCI microstructure cannot be considered as a ferritic ductile matrix with embedded holes.
3) The hypothesis of an internal interface inside the graphite elements due to the solidification process allows to describe the observed “onion-like” damaging micromechanism, although in the present simulation no mechanical properties gradient was considered. A further development of this work will consider also this gradient.

References

[1] C. Labrecque, M. Gagné, Ductile Iron: fifty years of continuous development, Canadian Metallurgical Quarterly. 37(5) (1998) 343-378.
[2] H. Morrogh, The solidification of Metals, The Iron and Steel Institute (1967) 238.
[3] T. Skaland, Nucleation mechanisms in ductile iron, in: Proceedings of the AFS Cast Iron Inoculation Conference, Schaumburg, Illinois. (2005) 13-30.
[4] M. J. Dong, C. Prioul, D. Francois , Damage Effect on the Fracture Toughness of Nodular Cast Iron : Part I . Damage Characterization and Plastic Flow Stress Modeling, Metall. Mater. Trans. A 28 (1997) 1997–2245.

[5] M. Cavallini, O. Di Bartolomeo, F. Iacoviello, Fatigue crack propagation damaging micromechanisms in ductile cast irons, Eng. Fract. Mech. 75 (2008) 694–704.
[6] F. Iacoviello, O. Di Bartolomeo, V. Di Cocco, V. Piacente, Damaging micromechanisms in ferritic–pearlitic ductile cast irons, Mater. Sci. Eng. A. 478 (2008) 181–186.
[7] V. Di Cocco, F. Iacoviello, M. Cavallini, Damaging micromechanisms characterization of a ferritic ductile cast iron, Eng. Fract. Mech. 77 (2010) 2016–2023.
[8] V. Di Cocco, F. Iacoviello, A. Rossi, Damaging micromechanisms characterization in a ferritic-pearlitic ductile cast iron, Fracture and Structural Integrity. 8 (2014) 62–67.
[9] V. Di Cocco, F. Iacoviello, A. Rossi, D. Iacoviello, D., Macro and microscopical approach to the damaging micromechanisms analysis in a ferritic ductile cast iron, Theor. Appl. Fract. Mech. 69 (2014) 26–33.
[10] S.Fintova, G.Anzelotti, R.Konecna, G.Nicoletto, Casting pore characterization by X-ray computed tomography and metallography, The archive of mechanical engineering, LVII (2010) 263-273.
[11] S.G.Lee, A.M.Gokhale, A.Sreeranganathan, Reconstruction and visualization of complex 3D pore morphologies in a high-pressure die-cast magnesium alloy, Material Science and Engineering. 427 (2006) 92-98.
[12] M.R.Baldissera, P.R.Rios, L.R.O. Hein, H.R.Z.Sandim, Three dimensional characterization of pores in Ti-6Al-4V alloy, Materials research. 14 (2011), 102-106.
[13] N.Chawla, V.V.Ganesh, Three-dimensional (3D) microstructure visualization and finite element modeling of the mechanical behaviour of heterogeneous materials, Microsc. Microanal. 11(2) (2005) 1642-1643
[14] J.Sauvola, M. Oietikainen, Adaptive document image binarization, Pattern recognition. 33 (2000) 225-236
[15] Q.Chen, Q.Sun, P.A.Heng, D.Xia, A double-threshold image binarization method based on edge detector, Pattern recognition. 41 (2008), 1254-1267.
[16] Singh et al 2011, Local Adaptive Automatic Binarization (LAAB), International Journal of Computer Application. 40, 6, (2012), 27-30
[17] N.Otsu, A threshold selection method from gray level histogram, IEEE Transactions on systems, man and cybernetics. 9 (1979) 62-66.
[18] V. Di Cocco, f. Iacoviello, D. Iacoviello, A. De Santis, Graphite nodules features identifications and damaging micromechanims in ductile irons, Fracture and Structural Integrity. 26 (2013) 12-21.